

Time-resolved X-ray powder diffraction on a three-way catalyst at the GILDA beamline

A. Martorana,^{a,b*} G. Deganello,^{a,b} A. Longo,^b
F. Deganello,^b L. Liotta,^b A. Macaluso,^a G. Pantaleo,^b
A. Balerna,^c C. Meneghini^{d,e} and S. Mobilio^{c,d}

^aDipartimento di Chimica Inorganica e Analitica 'Stanislao Cannizzaro', Università di Palermo, Viale delle Scienze, 90128 Palermo, Italy, ^bISMN-CNR, Sezione di Palermo, Via Ugo La Malfa 153, 90146 Palermo, Italy, ^cINFN-LNF, Via Enrico Fermi 44, 00044 Frascati, Italy, ^dDipartimento di Fisica 'E. Amaldi', Università di Roma Tre, Via della Vasca Navale 84, 00146 Roma, Italy, and ^eIstituto Nazionale per la Fisica della Materia-GILDA, BP 220, 38043 Grenoble CEDEX, France.
E-mail: cric2@unipa.it

Time-resolved X-ray diffraction experiments carried out at the beamline BM08-GILDA of ESRF allowed a study of the structural modifications taking place in a Pt/ceria-zirconia catalyst while the CO oxidation reaction was in progress. The capillary tube in which the sample is stored acts effectively as a chemical microreactor that ensures homogeneity of the sample treatments and minimization of diffusion effects. During the flowing of the reactant CO/He mixture, the investigated catalyst undergoes a fast Ce(IV)–Ce(III) partial reduction that involves the release of one O atom for every two reduced Ce cations. Because Ce(III) has a larger ionic radius than Ce(IV), the structural modification produces an increase of the lattice constant of the ceria-zirconia mixed oxide, and this increase is monitored by the translating imaging-plate device implemented at GILDA. The CO₂ resulting from the oxidation of the fluxed CO is monitored by a quadrupole mass spectrometer during the recording of the time-resolved X-ray diffraction pattern. The chemical and structural information was combined to show that the CO₂ yield is nearly constant until the catalytic system can provide oxygen for the reaction, while the structural rearrangement of the catalyst is delayed with respect to the switching on of the CO/He flux. After this induction time, during which CO₂ is produced with no structural modification of the catalyst, a fast increase of the lattice constant takes place.

Keywords: *in situ* X-ray diffraction; imaging plates; Rietveld; three-way catalysts; ceria-zirconia.

1. Introduction

Three-way catalysts (TWC) are materials tailored for the abatement of pollutants in gas exhausts of automotive vehicles. The triple task they are designed for – *i.e.* the reduction of nitrogen oxides and, simultaneously, the oxidation of carbon monoxide and of unburnt hydrocarbons – is best carried out in a narrow composition range of the reaction mixture (the so-called stoichiometric window) and at temperatures corresponding to a steady operation regime of the engine (Trovarelli, 1996). Outside these ideal conditions the catalyst performance can be far from optimal, thus considerable effort has been undertaken by industrial and academic researchers in order to develop new TWC systems with wider stoichiometric windows and effective temperature intervals.

CeO₂-based TWC systems are nowadays widely used and investigated because of the ability of Ce(IV) to undergo a straightforward

reduction to Ce(III) in a reductive environment and to be promptly reoxidized in an oxygen excess. The reduction of two Ce(IV) cations in the ceria network involves, to preserve the net charge neutrality, the release of one O atom, and the opposite oxidation process involves oxygen uptake from the reaction mixture. Therefore, while the actual catalyst for pollutants' redox reactions is constituted by the supported precious metals, the ceria-based promoter performs the fundamental task of keeping the gas exhaust composition within the stoichiometric window. The ability of ceria-based TWC systems to provide oxygen to the reaction environment can be improved by doping CeO₂ with different cations, such as Zr(IV) (Fornasiero *et al.*, 1995) and La(III) (Miki *et al.*, 1990; Deganello & Martorana, 2002), and supportation of the mixed oxide on γ - or η -alumina. As concerns, in particular, zirconium-doped ceria, it has been hypothesized that the oxygen mobility depends on the lattice deformation about the smaller Zr⁴⁺ cations (Vlaic *et al.*, 1997); a very accurate pulsed neutron diffraction study (Mamontov *et al.*, 2000) demonstrated the defective structure of the ceria-zirconia anion sublattice and ascribed the oxygen mobility to the noteworthy fraction of interstitial O atoms. Actually, while much work has been carried out to develop new TWC systems and to study their catalytic activity, further investigation of the structure-properties relationships could give useful indications for the tailoring of better materials. Time-resolved X-ray diffraction (XRD) studies, in particular, can provide interesting information about the structure of TWC systems in different temperatures and reaction environments. Pioneering work, in this respect, has been carried out by Ozawa & Loong (1999) on Zr- and La-doped ceria. These authors demonstrate that the Ce(IV) → Ce(III) reduction leads to an increase of the ceria-based mixed-oxide unit cell.

The apparatus for *in situ* XRD experiments at the BM08 GILDA beamline of the European Synchrotron Radiation Facility (ESRF) (Grenoble, France) (Meneghini *et al.*, 2001) is based on an IP (imaging plate) camera that can be used in translation mode. In this paper the improvement of the set-up for time-resolved experiments on catalytic systems is described and, as an example of application, the information obtained on a Pt/ceria-zirconia catalyst prepared by a sol-gel route is detailed. The sample is contained in a quartz capillary through which the gas reaction mixture is flowed. Using this geometry, the experimental conditions can be tuned to ensure that the reaction kinetics are not determined by the rate of diffusion of reactants and products but mostly by the chemical properties of the catalyst. Such a configuration of the reaction cell is particularly useful with TWC systems, because the rate of release of oxygen to the reaction environment is one of the most important parameters to be evaluated in the design of new materials.

2. Experimental

2.1. Time-resolved XRD set-up for catalytic applications

The experimental set-up for time-resolved XRD experiments at the GILDA beamline is described in a recently published paper (Meneghini *et al.*, 2001) and consists of a flat IP detector (200 × 400 mm) translating behind an adjustable-width Ta slit screen. The Ta slit system allows the recording of a narrow vertical portion of the Debye rings on the IP; successive XRD patterns ('strips') are collected during sample treatment on the translating IP. A gas-flux heater (Hot-air Blower, Cyberstar, Grenoble France) with remote temperature control allows the tuning of the sample temperature in the room temperature to 1223 K range.

A specific set-up has been implemented to monitor the structural evolution of a catalyst in the reaction environment. The sample is contained in a quartz capillary that is supported by an aluminium

frame fitted in a goniometer head. The capillary is open on both sides, which allows the reaction gases to be input at one end and the products to be conveyed to a quadrupole mass spectrometer (Thermostar GSD 300 T, Balzers) at the other end. As already pointed out (Clausen *et al.*, 1991), this geometry warrants the optimal experimental conditions as concerns (i) the absence of dead-sample volumes not reached by the gas flow, (ii) the uniformity of the sample temperature and (iii) the overcoming of diffusion effects. On the side of the structural analysis, the correspondence between the sample participating in the chemical reaction and that probed by the X-ray beam is therefore ensured. The layout of the reaction line and of the *in situ* X-ray diffraction is shown in Fig. 1. The bottles containing the gas mixtures are placed outside the experimental hutch, and the gas flow can be set to the most suitable values for the investigated reaction by proper tuning of the bottle manometer and a mass-flow controller (Brooks Instruments). The sample is kept fixed inside the capillary by quartz-wool frames on both the sides that prevent the powdered catalyst from polluting the quadrupole circuit.

The choice of the experimental conditions should take into account several contrasting factors: a large sample-to-detector distance and thin capillary diameter allow the line broadening to be reduced, but a shorter sample-to-IP distance permits the enlargement of the 2θ range and a larger diameter can be needed to ensure a stable gas flow through the sample. To guarantee the homogeneity of the temperature throughout the sample, the filled capillary length should be entirely under the jet of the blower, thus limiting the overall amount of catalyst that can be used in the experiment.

2.2. Sample preparation

The synthesis of the ceria–zirconia mixed oxide with nominal composition $\text{Ce}_{0.6}\text{Zr}_{0.4}\text{O}_2$ was carried out by a sol–gel procedure. The amounts of reagents (Aldrich, 99% analytical grade purity, used as delivered without any further purification) for the preparation of 5 g of ceria–zirconia promoter are given. The zirconium precursor [5.9 ml of $\text{Zr}(\text{OCH}_2\text{CH}_2\text{CH}_3)_4$, 70 wt% solution in *n*-propanol] was added at room temperature to $\text{Ce}(\text{NO}_3)_3 \cdot 6\text{H}_2\text{O}$ (8.5 g) dissolved in ethanol (20 ml). In order to promote the hydrolysis step determined by the crystallization water present in the cerium salt, the reaction temperature was raised from 298 to 338 K. The resulting mixture was stirred at 338 K overnight and gelation occurred in about 12 h. After evaporation to dryness in a vacuum, the material was calcined at 923 K for 8 h and subsequently at 1073 K for 1 h (heating rate 5 K min^{-1}).

The Pt catalyst (1 wt%) was prepared by impregnation of the ceria–zirconia oxide, which was characterized by a surface area of 48 $\text{m}^2 \text{g}^{-1}$, with a solution of $\text{Pt}(\text{acetylacetonate})_2$ in toluene at 343 K. After drying in a vacuum, the solid was calcined at 673 K for 5 h and then reduced at 623 K for 3 h (heating rate 1 K min^{-1}).

2.3. Sample treatments and experimental conditions

The investigated TWC sample was subjected to two types of thermal treatment: temperature ramps lasting 50 min from room temperature to 973 K and isothermal treatments for 60 min at 773 K. The ramps were carried out in pure He flux and in CO/He (0.1% vol). During the isothermal runs, the input gas was changed, after 10 min, from an oxidative O_2/He mixture (10% vol) to reductive (0.1% vol) CO/He. A 1 mm capillary diameter ensured a stable gas flow (5 ml min^{-1} at 2 atm measured at the bottle outlet) through the stored sample; the latter was obtained by sieving the catalyst and taking the particle-size fraction to be between 80 and 120 μm . A filled capillary length of about 1 cm was entirely bathed by the blow of the

heat gun, which was put at a distance of 1.5 mm from the capillary. The temperature effectively experienced by the sample was confirmed by the thermal expansion of a reference silver powder sample. With the above-quoted gas flux and sample amount, the resulting space velocity (given by the ratio between the gas flux and the catalyst volume) of 38197 h^{-1} was similar to typical values exploited in kinetic studies on macroscopic reactors.

Because of the presence of the input and output gas circuit and the hindrance of the aluminium frame that supports the capillary, it was not possible to spin the capillary during the time-resolved experiments. On the other hand, the samples were certainly isotropic, so that a satisfactory homogeneity of the scattered intensity was achieved. The chosen sample-to-IP distance was 155 mm, which ensured that, with the wavelength $\lambda = 0.72384 \text{ \AA}$, the most important part of the XRD pattern could be recorded. The instrumental line broadening (FWHM), which in flat IP geometry mainly depends on the values of the sample–detector distance and the capillary diameter (Norby, 1997), ranged between 0.36° at $2\theta = 10^\circ$ and 0.28° at $2\theta = 40^\circ$ (Meneghini *et al.*, 2001).

3. Results and discussion

The stable form of zirconia at room temperature is normally monoclinic, but the tetragonal form can be stabilized by impurities or small particle size (Lutterotti & Scardi, 1990). From a comparison of Figs. 2(a) and 2(b), which show, respectively, fragments of tetragonal zirconia, space group $P4_2/nmc$, and of cubic ceria, space group $Fm\bar{3}m$, it is clear that the two structures are very similar. The symmetry differs because cerium coordinates eight O^{2-} anions at the corners of a regular cubic box, while in the neighbourhood of zirconium two different Zr–O distances are actually present, which give rise to a somewhat distorted cubic coordination. If these two distances suitably degenerate into a single one and the ratio between the tetragonal lattice constants c_T and a_T is equal to $2^{1/2}$, tetragonal zirconia has the same symmetry as cubic ceria and can be referred to a cubic face-centred cell with volume $V_{\text{cub}} = 2V_T$, where $V_T = a_T a_T c_T$ is the tetragonal cell volume. It is likely, therefore, that ceria–zirconia solid solutions have an oxygen environment about the cations that is

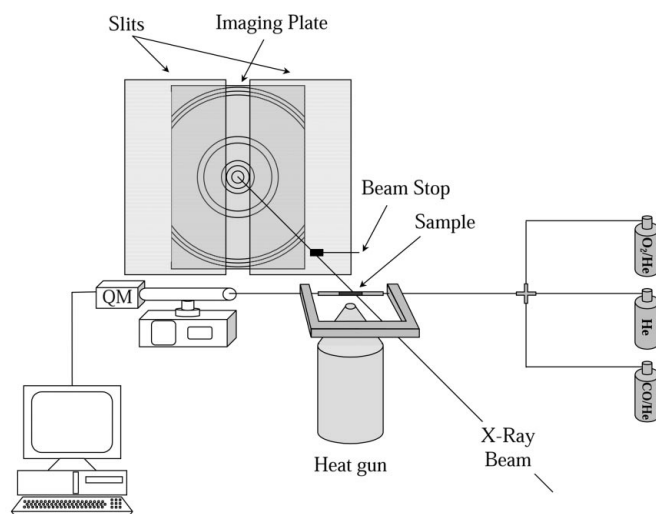


Figure 1
Schematic view of the experimental set-up developed at GILDA for time-resolved XRD experiments on TWC catalysts.

midway between the environment of the pure structures. Actually, as demonstrated by Vlaic *et al.* (1997), while Ce(IV) in a $\text{Ce}_{0.5}\text{Zr}_{0.5}\text{O}_2$ sample keeps the eightfold oxygen coordination, the number of O atoms about Zr(IV) is reduced to about six, with two anions at non-bonding distance that probably have higher mobility and are likely to contribute to the improvement of the redox properties of the material.

A typical XRD pattern of the investigated Pt/ceria–zirconia sample is reported in Fig. 3(a). The absence of any recognizable diffraction peak that could be associated with platinum-containing phases probably originates from both a small metal content and a very high dispersion. The diffraction pattern, as is particularly evident in the enlargement of Fig. 3(b), is consistent with the hypothesis that two very similar ceria–zirconia phases are present. In fact, the fitting performed by GSAS (Larson & Von Dreele, 1988), which involved

the weighted sum of a cubic ceria-like phase (from now on ‘cubic phase’) and a tetragonal zirconia-like phase (‘tetragonal phase’), gave good results, as can be estimated from inspection of the calculated and residual patterns reported in Figs. 3(a) and 3(b) and from the agreement factors reported in Table 1 (McCusker *et al.*, 1999). The cubic and tetragonal ceria–zirconias used in the fitting runs are likely to be representative of a continuous distribution of phases that are actually present in the investigated sample; clearly, the attempt to refine more than two phases would lead to severe correlations between the fitting parameters.

In Fig. 4 the dependence of the cell constant of the cubic phase, a_C , on the ramp temperature in CO/He 0.1% and pure He flux is shown. As already observed by Ozawa & Loong (1999) in a similar experiment, the CO/He ramp is very different from the corresponding He ramp: in the latter treatment the increase of a_C is essentially due to thermal expansion, whereas the larger a_C values in CO/He are a result of the reduction of Ce(IV) [ionic radius $r_{\text{Ce(IV)}} = 0.97 \text{ \AA}$] to

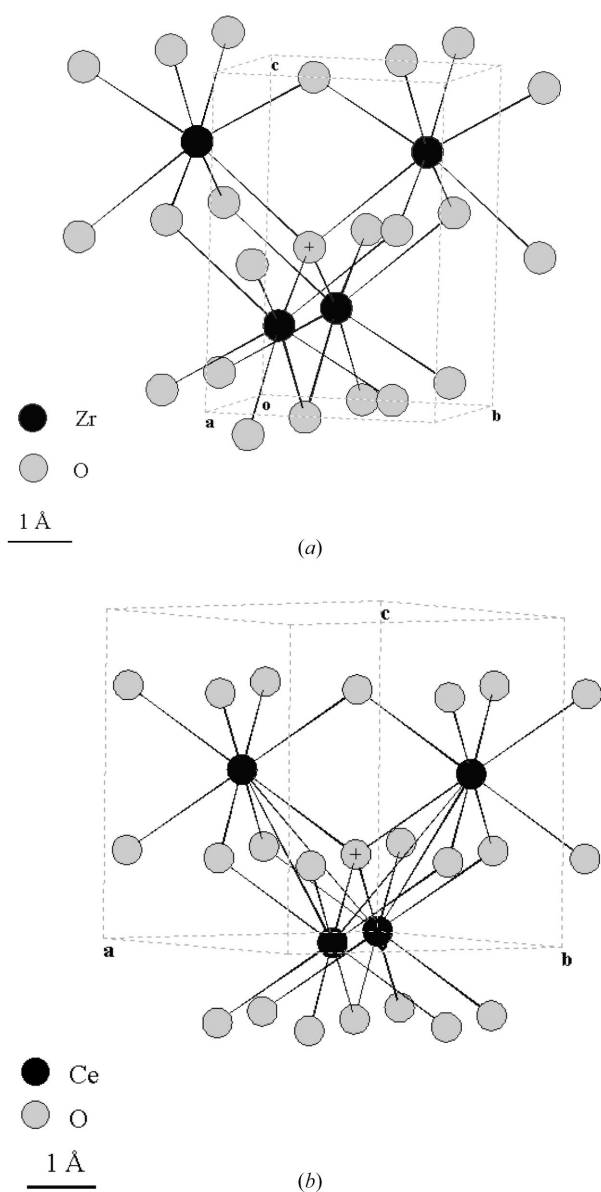


Figure 2
(a) Fragment of the structure of tetragonal zirconia. (b) Fragment of cubic ceria. The respective unit cells are shown by dashed lines.

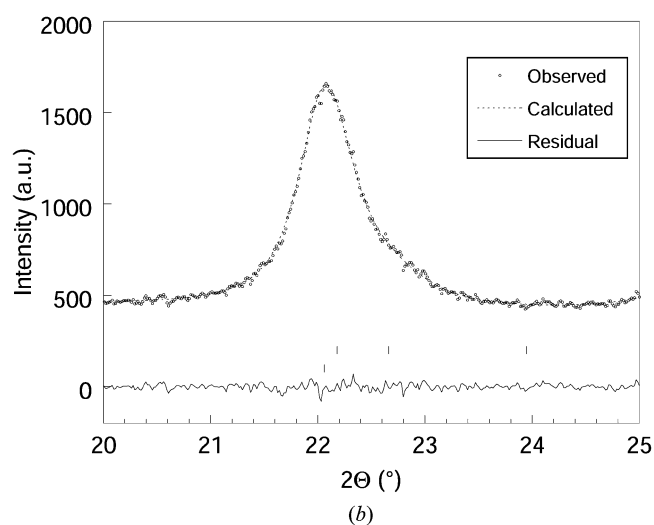
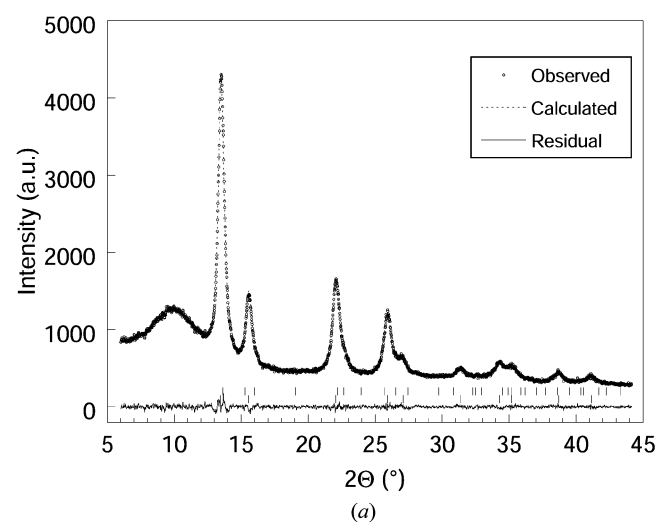


Figure 3
(a) Rietveld refinement of the ninth vertical strip of the imaging plate, corresponding to about 8 min of catalyst treatment at 773 K ($\lambda = 0.72384 \text{ \AA}$). Upper tick marks: tetragonal phase. Lower tick marks: cubic phase. The amorphous halo at $10^\circ 2\theta$ is due to the capillary scattering. (b) Enlargement of the $20\text{--}25^\circ 2\theta$ interval, demonstrating the presence of two phases.

Table 1
Agreement factors† of the Rietveld refinements.

Strip	$\chi^2‡$	$R_{wp}§$	$R_p¶$
3	0.90	4.50	3.39
8	0.88	4.13	3.10
13	0.86	4.13	3.10
18	0.91	4.19	3.16
23	0.94	4.21	3.22
28	0.95	4.27	3.23
36	0.91	4.12	3.13

† Sampled every five points in Figs. 5 and 6. ‡ $\chi^2 = \sum w(I_{obs} - I_{calc})^2 / (N_{obs} - N_{var})$.
§ $R_{wp} = 100[\sum w(I_{obs} - I_{calc})^2 / \sum w I_{obs}^2]^{1/2}$. ¶ $R_p = 100 \sum |I_{obs} - I_{calc}| / \sum I_{obs}$.

Ce(III) [$r_{Ce(III)} = 1.14 \text{ \AA}$]. A similar behaviour is shown by the tetragonal phase.

The refined value of the lattice parameter in the isothermal treatment at 773 K allowed the evaluation of the doping amount in the respective host lattices by the following procedure. The thermal expansion was determined from the increase of a_C versus T in the He ramp and used to discriminate between the thermal expansion effect and the expansion due to the reduction of Ce(IV). Assuming a linear dependence of a_C versus the amount of hosted species, the values obtained by the *GSAS* refinements were fitted using the equation (Kim, 1989)

$$a_C = 5.413 + \sum_k (2.2\Delta r_k + 0.15\Delta z_k) x_k, \quad (1)$$

where Δr_k is the difference between the ionic radius of the k th dopant and that of Ce(IV), Δz_k is the difference between the respective valencies, and x_k is the k th stoichiometric coefficient. Equation (1) allowed the determination of the amount of dopant Zr in the cubic phase of the fully oxidized Ce(IV)_{1-y}Zr_yO₂ sample and, assuming that the Zr content did not change in reductive conditions, was also applied to obtain the amount of Ce(III) in the reduced catalyst, according to the chemical formula Ce(IV)_{1-x-y}Ce(III)_xZr_yO_{2-x/2}.

In Fig. 5 the response of a_C to the change of the flowing mixture from O₂/He to CO/He at 773 K is shown; the reported a_C values were corrected for thermal expansion using the a_C values in the He ramp. The Zr doping fraction y was determined to be 0.25 from the lattice

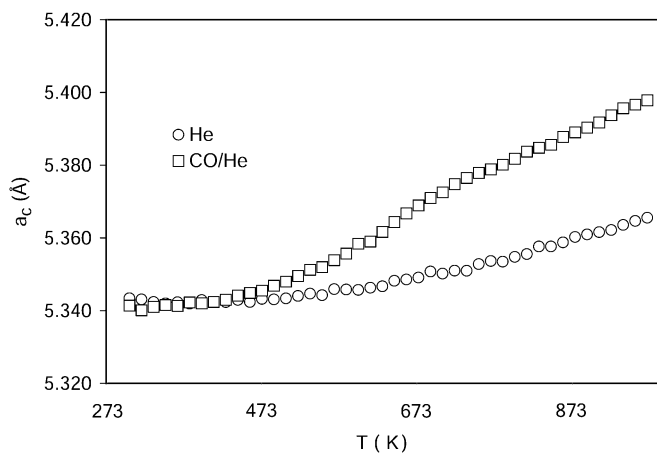


Figure 4
Lattice constant of the cubic phase versus treatment temperature in CO/He and He flux.

constant of the fully oxidized sample. This value was obtained by fitting equation (1) to the value $a_C = 5.34 \text{ \AA}$ (obtained from the room-temperature values of the He ramp, see Fig. 4), assuming that the Ce(III) content (x) was zero and, therefore, that the only dopant was Zr. About 5 min after the change of the reaction mixture from O₂/He to CO/He, a fast a_C increase takes place; afterwards, the a_C value keeps rising at a definitely slower rate. Assuming that the Zr content is not changed, the value of the lattice parameter is now fitted by varying x , the amount of Ce(III), in equation (1). The value $a_C \approx 5.36 \text{ \AA}$, which corresponds to the beginning of the slow increasing rate regime, is relative to the composition Ce(IV)_{0.67}Ce(III)_{0.08}Zr(IV)_{0.25}O_{1.96}; indeed, taking into account an uncertainty (evaluated from the scattering of neighbouring points in Fig. 5) of about 0.05% in the determination of the lattice parameter, the fraction of released oxygen is affected by a large error of about 10%. However, by inspection of Fig. 5 it is clear that the fluctuation of a_C before and after its steep rise is stable enough to ensure the reliability of Δa_C determined by the Rietveld refinement and, therefore, of the estimated amount of Ce(III) produced in the reaction.

The doping level and the amount of Ce(III) of the tetragonal phase were determined by a similar procedure, although the analysis can be only roughly quantitative, because the diffraction peaks are wider and overlapped, and there is also overlapping with the cubic phase peaks. On the basis of the structural similarity with the cubic component outlined above, a cubic equivalent cell parameter was calculated as

$$a_{\text{cub-eq}} = (2a_T a_T c_T)^{1/3},$$

and the same analysis as for the cubic phase was carried out. From Fig. 6 it is possible to establish that, despite the evident larger uncertainty in the $a_{\text{cub-eq}}$ parameter, the redox behaviour of the tetragonal component is very similar to that of the cubic phase, as concerns the delay time of the structural transition and the initial fast reduction followed by a slower formation of Ce(III). From the composition Ce(IV)_{0.42}Ce(III)_{0.10}Zr(IV)_{0.48}O_{1.95}, the observed tetragonality is clearly related to the noteworthy Zr amount. The fraction of Ce cations that underwent the Ce(IV) → Ce(III) transition is definitely higher than in the cubic phase, probably because the

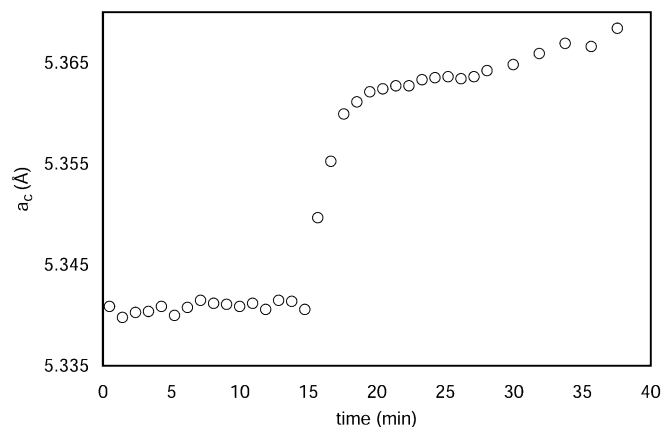


Figure 5
Lattice constant of the cubic phase versus time during the isothermal treatment of the catalyst at 773 K. At 10 min the gas mixture is switched from O₂/He to CO/He. Evidently the increase of a_C takes place with a delay of about 5 min with respect to the change of reaction environment.

smaller amount of cerium is more than balanced by a higher number of mobile O atoms (Vlaic *et al.*, 1997).

For both the cubic and the tetragonal phase, the weight fraction, which is determined in the Rietveld refinements of all the patterns, varies in the range 49–51% and is independent, as expected, of the oxidation state of ceria–zirconia. Assuming an equal weight composition of the cubic and tetragonal phase, the cerium and zirconium number fractions are, respectively, 0.63 and 0.37, which are very close to the input composition. As the synthesis procedure does not involve any loss of reagents, this result can be considered as further evidence of the reliability of the XRD analysis.

The CO₂ yield at 773 K is shown in Fig. 7. It is clear that the CO oxidation takes place immediately after the change of the reaction mixture from O₂/He to CO/He and remains nearly constant until the sample can release oxygen to the reaction environment. Conversely, the reduction of reticular Ce(IV) begins (see Figs. 5 and 6) with a definite delay with respect to the CO₂ production. Taking into account the overall quantity of converted CO and the amount of catalyst used in each experiment, the oxygen provided by the ceria–zirconia structure can account for about 80% of the converted CO.

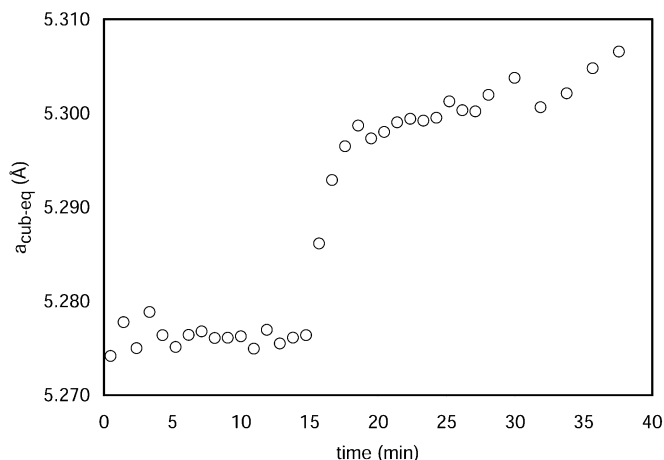


Figure 6 Cubic equivalent lattice constant of the tetragonal phase *versus* treatment time of the catalyst at 773 K. The behaviour is quite similar to that of the cubic phase.

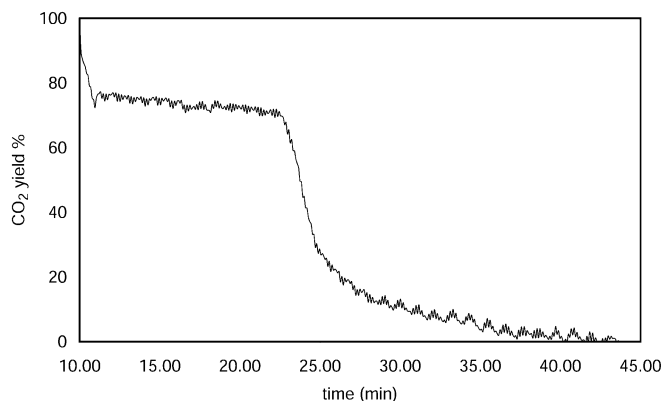


Figure 7 CO₂ yield of the catalyst in CO/He flux at 773 K, as determined by the mass spectrometry experiment carried out during the XRD experiment. Evidently the production of CO₂ begins immediately at 10 min treatment, after the change of reaction mixture to CO/He, and remains nearly constant until the catalyst can provide oxygen to the reaction environment.

The remaining 20% can be ascribed to the oxygen chemisorbed or physisorbed on the catalyst surface during the catalyst oxidation treatment. It appears, therefore, that initially a more readily accessible oxygen, probably coming from the support surface and/or chemisorbed on the platinum particles, is consumed. Only after this step does the depletion of surface oxygen produce the diffusion of bulk oxygen to the surface. Conversely, the rate of CO conversion does not present any significant variation in correspondence to the fast reduction of reticular Ce(IV), and the CO conversion continues after the fast Ce(IV) reduction process is finished. The experimental evidence is therefore that the reticular oxygen provided by the catalyst is in excess with respect to the need, while the rate of the reaction is determined by the process of CO oxidation.

The results of the structural analysis carried out on the time-resolved XRD data of the investigated ceria–zirconia samples are in qualitative agreement with those reported by Ozawa & Loong (1999) as concerns the cell expansion of ceria-based TWC systems in reductive environments. However, although a direct comparison cannot be performed, because the materials (Ce_{0.1}Zr_{0.9}O₂/Pt 0.1%) and the reaction conditions are different, it is noteworthy that the time scale of the structural rearrangement is very different [only a few minutes in the experiments described in this paper, *versus* several hours for those of Ozawa & Loong (1999)] and that no delay in the structural variation is reported by Ozawa & Loong (1999). Taking into account that their experiment was performed on a sample obtained by compacting a powder into a tablet and putting it in a chamber with controlled atmosphere, it cannot be excluded that under such conditions the response of the material is mainly ruled by the time necessary for the reaction mixture and the products to completely diffuse through the bulk of the sample and that the recorded time-resolved patterns are actually an average of contributions from volumes of the sample in different oxidation states.

4. Conclusions

A set-up for the time-resolved XRD analysis of heterogeneous catalysts operating in the gas phase was developed at GILDA. The apparatus was used for the first time to study TWC systems composed of 1 wt% Pt supported on ceria–zirconia mixed oxide. The information that could be extracted from this kind of experiment has been shown. In particular, the geometry of the apparatus is best suited for performing *in situ* experiments, as the set-up overcomes possible diffusion problems of devices projected with a different operational scheme. The use of the translating imaging plate allows the fast recording of the whole diffraction pattern and very good counting statistics; a drawback of this geometry is the lower resolution with respect to point detector diffractometers, in particular when large capillary diameters must be used to ensure a stable gas flow. New experiments have been carried out at GILDA (the data are presently being analysed) using a chemically inert α -alumina diffraction standard mixed with the catalyst to improve the accuracy in the determination of the lattice constants. The investigation of lower temperatures and different reaction mixtures will hopefully provide further information about the structure–properties relationships in these materials.

This study has been carried out with the financial support of the MURST projects *CLUSTER 20P5* and *Catalysts for the removal of nitrogen oxides in lean burn engine emissions*. The experimental set-up for the simultaneous monitoring of the chemical reaction and the XRD patterns could not have been implemented without the

precious collaboration of the GILDA technicians Fabio D'Anca, Franco Campolungo, Vittorio Sciarra and Vinicio Tullio.

References

- Clausen, B. S., Steffensen, G., Fabius, B., Villadsen, J., Feidenhans, L. R. & Topsøe, H. (1991). *J. Catal.* **132**, 524–535.
- Deganello, F. & Martorana, A. (2002). *J. Solid State Chem.* **163**, 527–533.
- Fornasiero, P., Di Monte, R., Ranga Rao, G., Kaspar, J., Meriani, S., Trovarelli, A. & Graziani, M. (1995). *J. Catal.* **151**, 168–177.
- Kim, D. (1989). *J. Am. Ceram. Soc.* **72**, 1415–1421.
- Larson, A. & Von Dreele, R. B. (1988). Report LAUR 86-748. Los Alamos National Laboratory, Los Alamos, NM, USA.
- Lutterotti, L. & Scardi, P. (1990). *J. Appl. Cryst.* **23**, 246–252.
- McCusker, L. B., Von Dreele, R. B., Cox, D. E., Louër, D. & Scardi, P. (1999). *J. Appl. Cryst.* **32**, 36–50.
- Mamontov, E., Egami, T., Brezny, R., Koranne, M. & Tyagi, S. (2000). *J. Phys. Chem. B*, **104**, 11 110–11 116.
- Meneghini, C., Artioli, G., Balerna, A., Gualtieri, A. F., Norby, P. & Mobilio, S. (2001). *J. Synchrotron Rad.* **8**, 1162–1166.
- Miki, T., Ogawa, T., Haneda, M., Kakuta, N., Ueno, A., Tateishi, S., Matsuura, S. & Sato, M. (1990). *J. Phys. Chem.* **94**, 6464–6467.
- Norby, P. (1997). *J. Appl. Cryst.* **30**, 21–30.
- Ozawa, M. & Loong, C.-K. (1999). *Catal. Today*, **50**, 329–342.
- Trovarelli, A. (1996). *Catal. Rev. Sci. Eng.* **38**, 439–519.
- Vlaic, G., Fornasiero, P., Geremia, S., Kaspar, J. & Graziani, M. (1997). *J. Catal.* **168**, 386–392.